



1 **Future projections of daily hazy and clear weather conditions over the North China**

2 **Plain using a Perturbed Parameter Ensemble**

3 Shipra Jain¹, Ruth M. Doherty¹, David Sexton², Steven Turnock^{2,3}, Chaofan Li⁴, Zixuan Jia¹,

4 Zongbo Shi⁵, Lin Pei⁶

5 ¹School of GeoSciences, The University of Edinburgh, Edinburgh, United Kingdom

6 ²Met Office Hadley Centre, Exeter, United Kingdom

7 ³University of Leeds Met Office Strategic (LUMOS) Research Group, School of Earth and
8 Environment, University of Leeds, UK

9 ⁴Center for Monsoon System Research, Institute of Atmospheric Physics, Chinese Academy of
10 Sciences, China

11 ⁵School of Geography, Earth and Environmental Sciences, University of Birmingham,
12 Birmingham, United Kingdom

13 ⁶Institute of Urban Meteorology, China Meteorological Administration, Beijing, China

14

15 **Corresponding Author:** Shipra Jain (Shipra.Jain@ed.ac.uk)



16 **Abstract**

17 We examine past and future changes in both winter haze and clear weather conditions over the
18 North China Plain (NCP) using a Perturbed Parameter Ensemble (PPE) and elucidate the
19 influence of model physical parameterizations on these future projections for the first time. We
20 use a meteorology-based Haze Weather Index (HWI), which was developed to examine the
21 haze conducive weather conditions for Beijing. We find that the HWI can be used as an
22 indicator of winter haze across the entire NCP due to the extended spatial coherence of the
23 local meteorological conditions. The PPE generated using the UK Met Office HadGEM-GC3
24 model shows that under a high-emission (RCP8.5) scenario, the frequency of haze conducive
25 weather is likely to increase whereas the frequency of clear weather is likely to decrease in
26 future. However, a change of opposite sign with lower magnitude in the frequencies, though
27 less likely, is also possible. In future, the total number of hazy days for a given winter can be
28 as much as ~3.5 times higher than the number of clear days over the NCP. We also examined
29 the changes in the interannual variability of the frequency of hazy and clear days and find no
30 marked changes in the variability for future periods. The future frequencies of winter hazy and
31 clear days in the PPE are largely driven by changes in zonal-mean mid-tropospheric winds and
32 the vertical temperature gradient over the NCP. We do not find any discernible influence of
33 model physical parameterizations on the future projections of trends in the frequency of hazy
34 or clear days. We find a clear impact of anthropogenic climate change on future trends for both
35 hazy and clear days, however, it is only discernible for specific periods due to the large
36 underlying internal variability in the frequencies of hazy and clear days.



37 **1. Introduction**

38 Over the last decade, a number of severe haze episodes (several days or longer) were
39 reported over the North China Plain (NCP) during boreal winter (December-January-February,
40 DJF). In January 2013, unprecedented PM_{2.5} levels exceeding 450 µg m⁻³ were observed over
41 the NCP (Wang et al., 2014a; Wang et al., 2014b; Zhang et al., 2018; Zhang et al., 2013).
42 Similar events were also observed in November-December 2015 when the PM_{2.5} concentrations
43 reached as high as 1000 µg m⁻³ in Beijing and caused the first-ever ‘red alert’ for severe air
44 pollution (Liu et al., 2017; Zhang et al., 2017). In December 2016, around 25% of the land area
45 of China was covered with severe haze for around one week (Yin and Wang, 2017). These
46 severe haze events adversely impacted public health including mortality, visibility, and
47 ultimately the economy of the country (Bai et al., 2007; Chen and Wang, 2015; Kan et al.,
48 2012; Kan et al., 2007; Wang et al., 2006; Xu et al., 2013; Hong et al., 2019).

49 Previous research has shown that the persistence of severe haze for days during winters
50 over the NCP occurred due to the combined effect of local and regional high pollutant
51 emissions and stagnant meteorological conditions (Li et al., 2018; He et al., 2016; Jia et al.,
52 2015; Pei et al., 2018; Zhang et al., 2021). The normal winter meteorological conditions over
53 the NCP are characterized by northwesterly flow near the surface through to the mid-
54 troposphere associated with the East Asian winter monsoon (An et al., 2019; Renhe et al., 2014;
55 Li et al., 2016; Xu et al., 2006). However, during the severe haze episodes, the mid-tropospheric
56 trough was reported to be shallower and shifted northwards leading to a weaker than normal
57 northwesterly flow and reduced horizontal transport of air pollutants from the NCP (Chen and
58 Wang, 2015). The weaker northwesterlies near the surface also reduces the intrusion of cold
59 and clean air from the high-latitudes to the NCP (Xu et al., 2006). In addition to changes in
60 horizontal winds, the vertical temperature gradient between the lower and upper troposphere
61 over the NCP enhances the thermal stability and reduces atmospheric mixing leading to the



62 build-up of the atmospheric pollutants over this region (Hou and Wu, 2016; Sun et al., 2014;
63 Wang et al., 2014a; Zhang et al., 2018; Cai et al., 2018). The planetary boundary layer height
64 is also found to be suppressed during extreme haze events leading to accumulation of
65 pollutants, notably PM_{2.5} concentrations (Liu et al., 2018; Petäjä et al., 2016), due to an increase
66 in moisture, reduced vertical mixing and dispersion which aids aerosol growth during high haze
67 events over the NCP (An et al., 2019; Tie et al., 2017).

68 In this paper, our focus is on the meteorological driven changes leading to daily hazy
69 or clear weather conditions over the NCP. On a daily scale, recent studies suggest an increase
70 in the occurrence of large-scale meteorological conditions favourable for winter haze over the
71 NCP under climate change. Cai et al. (2017) used a meteorology-based daily Haze Weather
72 Index (HWI) and projected a 50% increase in the frequency of winter haze conducive weather
73 conditions, similar to the January 2013 event, over Beijing in the future (2050-2099) as
74 compared to the historical (1950-1999) period under RCP8.5 scenario using 15 CMIP5 models.
75 Han et al. (2017) also examined indicators of haze pollution potential (e.g. horizontal transport,
76 wet-deposition, ventilation conditions) using three regional climate simulations and projected
77 a higher probability of haze pollution risk over Beijing-Tianjin-Hebei region under the RCP4.5
78 scenario. Liu et al. (2019) projected a 6-9% increase in the winter haze frequency under 1.5°
79 and 2° global warming, respectively based on 20 CMIP5 models. Qiu et al. (2020) also projected
80 an increase of 21% and 18% in severe winter haze episodes under 1.5° and 2° global warming,
81 respectively using an ensemble of climate simulations from the Community Earth System
82 Model 1 (CESM1) for a low warming experiment (Kay et al., 2015). Callahan and Mankin
83 (2020) found 10-15% increase in winter hazy days in CMIP5 multimodel and CESM large
84 ensemble under 3° warming and emphasized a large influence of internal variability in addition
85 to anthropogenic forcing on future haze conducive weather over Beijing. A few studies also
86 find little impact of climate change on future projections of haze (Shen et al., 2018; Pendergrass



87 et al., 2019), which could partly arise due to the under-sampling of internal variability
88 associated uncertainty in their projections (Callahan and Mankin, 2020), as well as model-to-
89 model differences. Hence, there is a large uncertainty as to how haze conducive weather
90 conditions may change in the future and these depend on haze metric or underlying processes
91 considered for projections.

92 In order to account for the uncertainty in the future projections (e.g. of large-scale
93 circulation) particularly at the regional scale (Hawkins and Sutton, 2012; Deser et al., 2012;
94 Deser et al., 2014), it is desirable to use an ensemble of climate change simulations. Whilst a
95 multimodel ensemble, e.g. CMIP5 or CMIP6, is commonly used for climate change studies,
96 several other studies have also emphasised the use of an initialised ensemble or Perturbed
97 Parameter Ensemble (PPE) from a single model to assess the uncertainties and obtain a
98 comprehensive range of possible future climate realisations for the same emission scenario for
99 a given model (Knutti et al., 2010). All three methodologies have different advantages. For
100 instance, using multiple models allows us to sample structural uncertainty in future projections,
101 which cannot be sampled using a single model. On the other hand, using an initialised ensemble
102 from a single model allows us to sample a broader range of internal variability, which is often
103 under-sampled in a multimodel ensemble. The advantage of using the PPE over the initialised
104 or multimodel ensemble is that it not only accounts for internal variability but also model
105 uncertainty arising due to the different settings of the physical parameterisations in a single
106 model.

107 Both multimodel ensemble and initialised ensemble from a single model have been
108 used to assess the future winter haze conducive conditions over Beijing. In this paper, we use
109 a PPE generated using the UK's Met Office HadGEM-GC3 model to assess for the first time
110 the impact of both model physical parameterisations and anthropogenic climate change on
111 future daily haze conducive weather conditions using the HWI. We first determine the spatial



112 extent for which the HWI can be used as an indicator of air quality over China (Section 3). We
113 examine the changes in the frequency of hazy and clear days for historical and three future
114 periods, i.e. near (2006-2032), mid (2033-2059) and far (2060-2086) future, over the NCP
115 (Section 4). We also analyse the changes in the interannual variance of the frequency of hazy
116 and clear days for the future periods as compared to the historical (Section 5). We investigate
117 the importance of the different meteorological variables used in the HWI in determining the
118 future changes in haze conducive conditions in the PPE (Section 6). Finally, we assess the
119 model physical parametrisations and anthropogenic climate change on the frequency of future
120 hazy and clear weather conditions over the NCP (Section 7). More details on the data and
121 methods used in this paper are provided in the next section.

122 **2. Data & Methods**

123 **2.1 Observations, Reanalysis Outputs and PPE Model Simulations**

124 Hourly $PM_{2.5}$ concentrations are used from the US embassy site for Beijing for DJF
125 from 2009-2017. Daily mean $PM_{2.5}$ concentrations are constructed using hourly data to identify
126 hazy and clear days and evaluate the performance of the HWI for Beijing (see Section 3). We
127 also used newly released gridded daily $PM_{2.5}$ concentrations for DJF from Chinese Air Quality
128 Reanalysis Datasets (CAQRA) provided by China National Environment Monitoring Centre
129 for 2013-2017 (Kong et al., 2021) to test the performance of the HWI across entire China. The
130 CAQRA data has been produced by assimilating surface air quality observations from over
131 1000 monitoring sites in China and is available at a high spatial resolution of around 15×15 km
132 and hourly temporal resolution over China. More details on the validation of the CAQRA
133 dataset against the independent station data is provided in (Kong et al., 2021). The visibility
134 data for Beijing (homogenized data for 20 stations in Beijing) is provided by the National



135 Meteorological Information Center of China, Chinese Meteorological Agency for DJF 1999-
136 2018.

137 We used daily ERA-5 reanalysis data of four variables: meridional wind at 850 hPa
138 pressure level (V_{850}), zonal wind at 500 hPa pressure level (U_{500}), temperatures at 850 hPa
139 level (T_{850}) and 250 hPa (T_{250}) to calculate the HWI for DJF 1979-2019. The ERA-5 data used
140 here is available at $0.25^\circ \times 0.25^\circ$ horizontal resolution and hourly temporal resolution
141 (Hersbach et al., 2020).

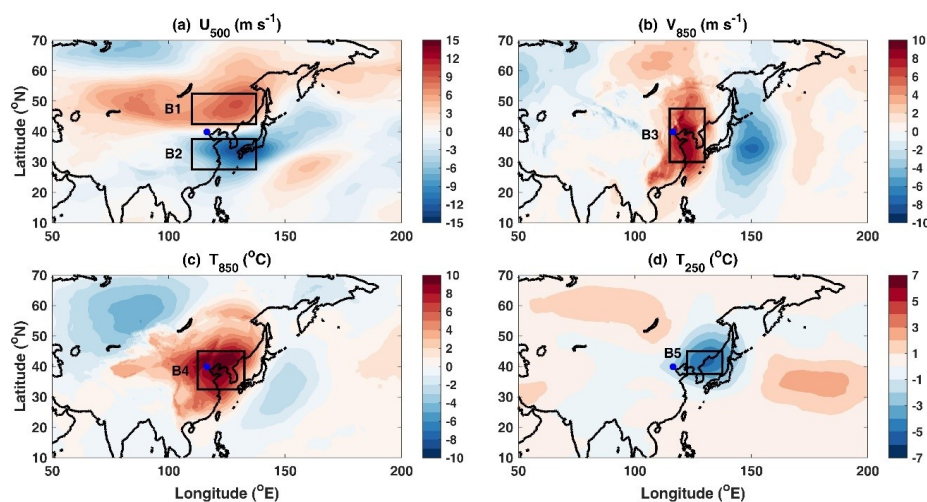
142 We used a PPE of climate simulations produced using the recent configuration of the
143 UK Met Office's HadGEM3-GC3.05 coupled model (Sexton et al., 2021; Yamazaki et al.,
144 2021). The base model used for PPE, HadGEM3-GC3.05, has a horizontal resolution of ~ 60
145 km with 85 vertical levels. A total of 47 model parameters from seven parameterization
146 schemes were simultaneously perturbed to obtain the PPE (the full list of perturbed parameters
147 is provided in Table 1 of (Sexton et al., 2021). Here, we used daily outputs of V_{850} , U_{500} , T_{850}
148 and T_{250} for DJF for the historical (1969-2005) and future (2006-2089) under the RCP8.5
149 scenario. In addition, we also assessed internal variability using 200-year control simulations
150 for each PPE member where 1900 boundary conditions were prescribed. Overall, 16 PPE
151 members are available for all the control, historical and RCP8.5 simulations.

152 2.2 Calculation of the HWI

153 We analyse the composite differences in the U_{500} , V_{850} , T_{850} and T_{250} for hazy ($PM_{2.5}$
154 concentrations $> 150 \mu\text{g m}^{-3}$) and clear ($PM_{2.5}$ concentrations $< 35 \mu\text{g m}^{-3}$) days across China
155 for DJF 2009-2017 (Fig. 1) (see next section for the cut-offs values used for $PM_{2.5}$
156 concentration). Figure 1 shows the difference in the zonal wind speed with a dipole pattern
157 suggesting a northward shift in the mid-tropospheric trough (Fig. 1a), weakened northerly flow
158 (Fig. 1b), higher temperatures in the lower troposphere and lower temperatures in the upper



159 troposphere (Fig. 1c-d) over the NCP during hazy days as compared to the clear days. These
160 findings are consistent with the previous studies (e.g. Cai et al., 2017) that showed similar
161 changes in these meteorological variables. Cai et al. (2018) have examined the use of other
162 variables such as geopotential height, boundary layer thickness and local stratification
163 instability and do not find any significant differences in the performance of HWI by inclusion
164 of more weather parameters. Therefore, we also use only these four variables for our analysis.



165

166 **Figure 1** Winter composites of differences in (a) u-wind at 500 hPa level (U_{500}) (b) v-wind at
167 850 hPa level (V_{850}) (c) temperature at 850 hPa level (T_{850}) and (d) temperature at 250 hPa
168 level (T_{250}) over China for all available days with high $PM_{2.5}$ ($>150 \mu\text{g m}^{-3}$) and low $PM_{2.5}$
169 ($<35 \mu\text{g m}^{-3}$) concentration for DJF 2009-2017 for the US embassy station for Beijing. The
170 blue dot shows the location of Beijing. Red colour in (a) and (b) shows strengthened westerlies
171 and weakened northerlies, respectively.

172 The winter HWI is calculated using the methodology given by Cai et al. (2017). For the
173 observational HWI, we use ERA-5 reanalysis data for the period 1979-2019. We first create a
174 daily DJF time series of each variable for each reanalyses grid point over China. The daily DJF
175 time series is concatenated for the period 1979-2019. A daily standardised anomaly time series
176 is created for each meteorological variable by first removing the daily mean climatology from
177 each day of the time series and then normalising by the standard deviation. Spatial averages



178 are then obtained over the relevant boxes (B1 to B5) for each meteorological variable following
179 Cai et al. (2017) (Fig. 1). The HWI time-series is calculated by using the following equation:

$$180 \quad \text{HWI}(t) = U_{500}(t) + V_{850}(t) + dT(t)$$

181 where $U_{500} = U_{500,B1}(t) - U_{500,B2}(t)$, $V_{850} = V_{850,B3}(t)$, and $dT = T_{850,B4}(t) - T_{250,B5}(t)$. The HWI
182 (t) time series is then itself normalized by its own standard deviation.

183 For the PPE historical and RCP8.5 simulations, the daily HWI time series is calculated
184 for each ensemble member for DJF for 1969-2089 using the same methodology as used for
185 ERA-5, with the difference being that the normalisation of the PPE time-series (1969-2089) is
186 performed using the historical standard deviation (1969-2005), following Cai et al. (2017).
187 Similarly, the HWI time series is calculated for the PPE pre-industrial control simulations for
188 170 model years out of 200 model years (first 30 years are discarded as model spin-up period).
189 The normalisation of the pre-industrial control time series is performed using the standard
190 deviation for 170 years. The pre-industrial control simulations used here are initialised with
191 past forcings corresponding to the year 1900 and therefore are an approximate representative
192 of the internal variability of the current climate as this does not take into account any temporal
193 changes in the internal variability from 1900 to the historical and future periods used here.

194 **3. Relationship between the Haze Weather Index and air quality indicators**

195 We determine the relationship between HWI and $PM_{2.5}$ concentration for Beijing. As
196 visibility is an optical representative of haze (Wang et al., 2006) and available for a relatively
197 long period (1999-2018) as compared to the $PM_{2.5}$ concentrations, we also correlate the HWI
198 with the visibility over Beijing. We then test the relationship between HWI and $PM_{2.5}$
199 concentrations over entire China to determine the spatial extent of the region for which HWI
200 can be used as an indicator of air quality. We use the 25th and 75th percentile values of daily
201 mean $PM_{2.5}$ concentrations to identify the clear and hazy days, respectively for each dataset.



202 For visibility, we use the opposite criterion, i.e. 25th percentile as a threshold for hazy days and
203 75th percentile as a threshold of clear days, as lower visibility is associated with hazy days and
204 higher visibility with clear days. The days with daily PM_{2.5} concentration or visibility lying
205 between the 25th and 75th percentile values are identified as moderately polluted days.

206 **3.1 PM_{2.5} concentrations for Beijing versus HWI**

207 Figure 2 (a) shows that the daily HWI increases linearly with increasing PM_{2.5}
208 concentrations for up to ~150 µg m⁻³ and for PM_{2.5} > 150 µg m⁻³, the HWI starts to level-off
209 (note the log scaling in the y-axis). The time-series correlation between the HWI and PM_{2.5}
210 concentration is ~0.58, which is significant at the 1% level. Callahan et al. (2019) have also
211 obtained a correlation coefficient of 0.58 for daily PM_{2.5} concentrations from the U.S. embassy
212 in Beijing and the HWI calculated using NCAR R1 reanalysis.

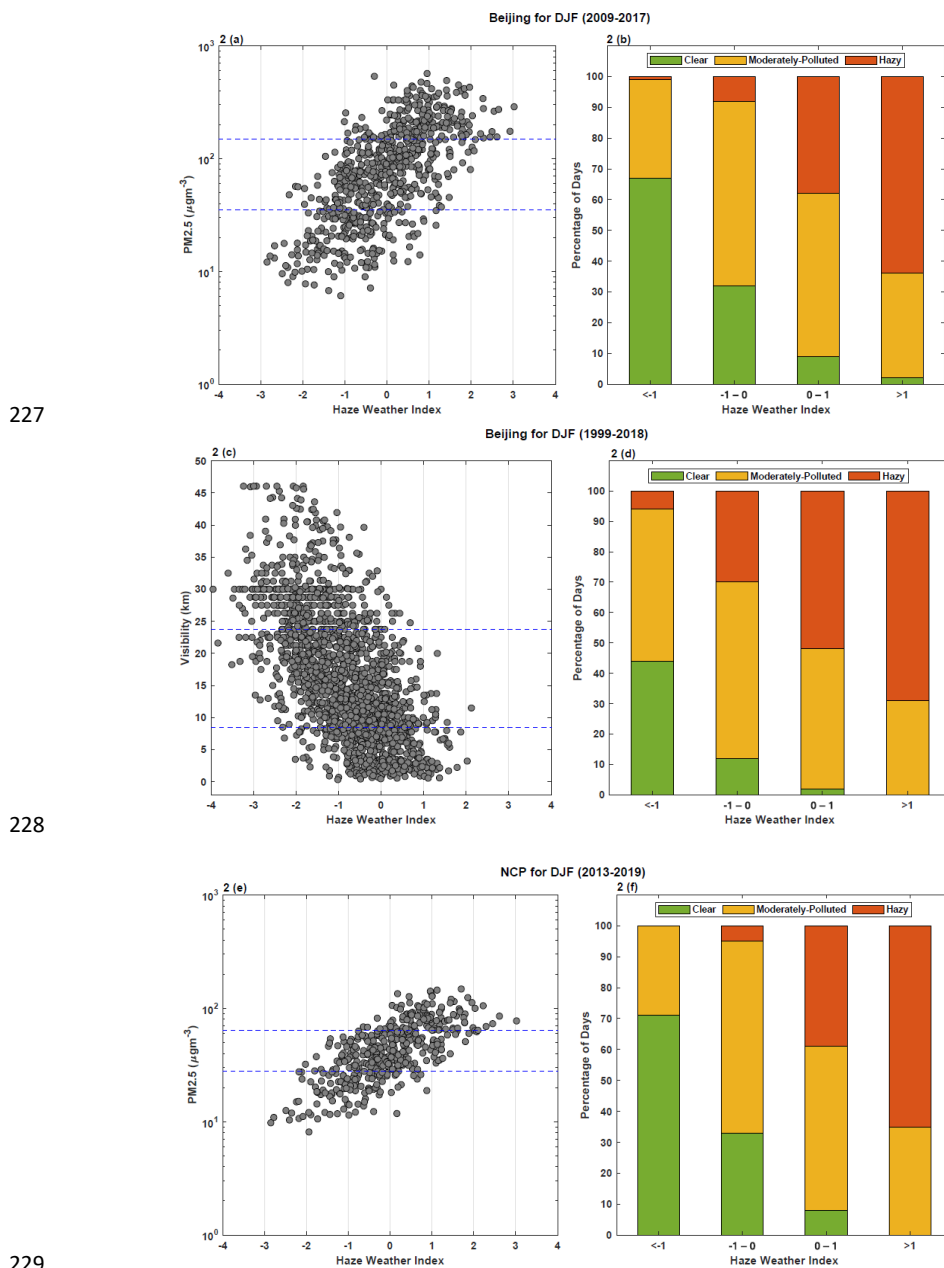
213 The 25th and 75th percentile values of daily mean PM_{2.5} concentrations for the US
214 embassy Beijing station for DJF 2009-2017 are ~35 and ~150 µg m⁻³ respectively. We
215 determine the percentage of hazy days (with daily mean PM_{2.5} concentrations >150 µg m⁻³) and
216 clear days (with daily mean PM_{2.5} concentrations < 35 µg m⁻³) for different HWI ranges (Fig.
217 2b). Out of all days with HWI >1, 64% have daily mean PM_{2.5} concentrations > 150 µg m⁻³ and
218 98% with PM_{2.5} concentrations >35 µg m⁻³. This suggests that for HWI >1, almost all days are
219 hazy or moderately polluted. Similarly, almost all days with HWI < -1 are clear or moderately
220 polluted. Using HWI thresholds of ±1 demarcates between the clear and hazy days, i.e. almost
221 no clear days occur for HWI >1 and almost no hazy days occur for HWI < -1.

222 **3.2 Visibility for Beijing versus HWI**

223 Figure 2 (c) shows that the HWI is inversely related to the visibility for the Beijing
224 station. The time-series correlation between the HWI and visibility is -0.63, which is significant



225 at the 1% level. The days with visibility < 8.5 km are identified as hazy days, days with
226 visibility > 23.8 km are identified as clear days. For days with HWI > 1 , no clear days occur



230 **Figure 2 (a)** Daily mean PM_{2.5} concentrations versus HWI and **(b)** percentage of clear, moderately
231 polluted and hazy days for different HWI ranges for the US embassy Beijing station for DJF 2009-

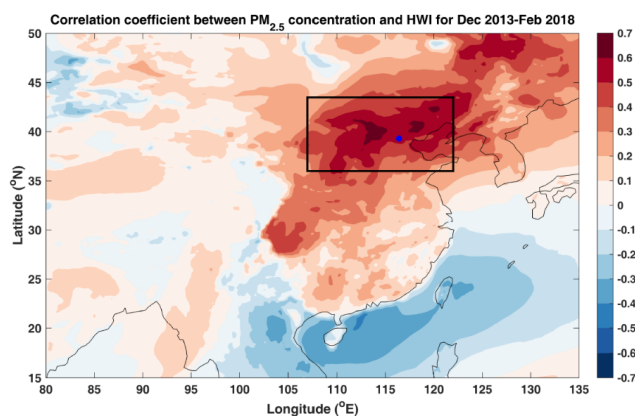


232 2017. (c) Daily mean visibility versus HWI and (d) percentage of clear, moderately polluted and hazy
233 days for different HWI ranges for the Beijing stations for DJF 1999-2018. (e) Daily mean PM_{2.5}
234 concentrations versus HWI and (f) percentage of clear, moderately polluted and hazy days for different
235 HWI ranges for the NCP for DJF 2009-2017. Blue lines show the 25th and 75th percentile thresholds
236 used to define clear and hazy days for each dataset.

237 and similarly for days with HWI < -1, only 6% of days are hazy (Fig 2d). This further confirms
238 that the correlation between the HWI and haze is significant for a longer period (1999-2018)
239 using visibility as a metric for haze (alternative to the PM_{2.5} concentrations used above).

240 3.3 PM_{2.5} concentrations over North China Plain versus HWI

241 We now determine the spatial extent for which HWI can be used as an indicator of
242 PM_{2.5} concentrations using data from CAQRA reanalysis. We correlate the daily time-series of
243 PM_{2.5} concentration at each grid point with the HWI for DJF 2013-2017 (Fig. 3). Over the
244 entire NCP (36-43.5 °N, 107-122 °E), the correlation coefficient between the daily HWI and
245 gridded PM_{2.5} concentration is ~0.7, significant at the 1% level. The correlation is considerably
246 lower but still significant over other eastern China regions, e.g. north easternmost China and
247 the Sichuan Basin (27-32 °N, 102-107 °E).



248
249 **Figure 3** Spatial distribution of correlation between winter PM_{2.5} concentrations and HWI time series
250 at each grid point. Blue dot shows the Beijing station (39.3 °N, 116.4 °E) and the black rectangle shows
251 the North China Plain (36-43.5 °N, 107-122 °E).

252 Considering daily mean PM_{2.5} concentrations averaged over the NCP, we also find a
253 linear relationship with the daily HWI ($r = 0.66$; significant at the 1% level; Fig 2e). The values



254 of $PM_{2.5}$ concentrations for NCP are lower as compared to the station values of $PM_{2.5}$
255 concentrations at the US Embassy Beijing and the correlation coefficient is higher. This could
256 be due to the different time periods for the two dataset, i.e. 2009-2017 for the US embassy and
257 2013-2017 for the CAQRA reanalyses, and spatial averaging of $PM_{2.5}$ concentrations over the
258 NCP region. We also calculate the percentage of clear and hazy days for different HWI ranges
259 for the larger domain of the NCP using the 25th and 75th percentile values, respectively. The
260 percentage of hazy and clear days for $HWI > 1$ and $HWI < -1$ for NCP in CAQRA reanalyses
261 are very similar to the values obtained for the US embassy Beijing station (Fig 2f).

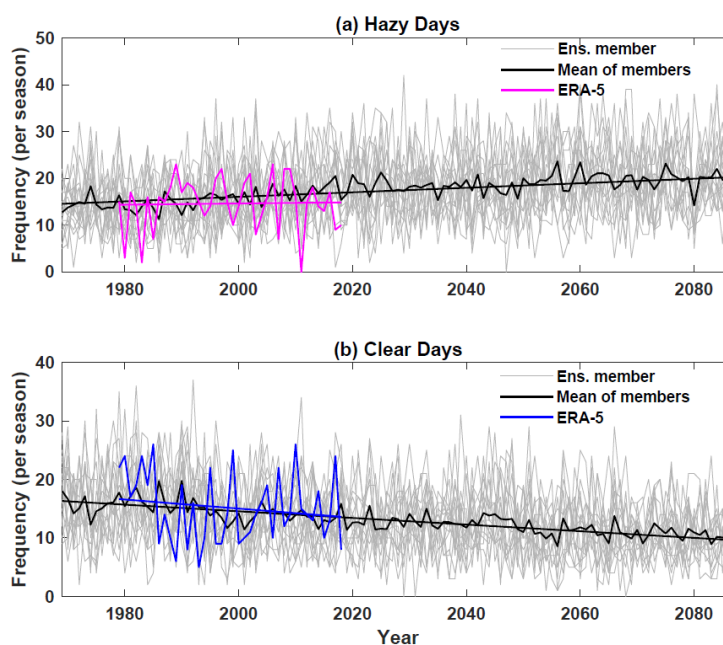
262 Overall, our results confirm that the daily HWI has a robust relationship with daily
263 $PM_{2.5}$ concentrations not only for the Beijing station but across the NCP for the given time
264 periods. Therefore, we use $HWI > 1$ as a threshold for hazy days and $HWI < -1$ as a threshold
265 of clear days across the NCP region. This threshold is also consistent with several other studies
266 (e.g., Cai et al., 2017; Callahan and Mankin, 2020; Callahan et al., 2019), that have used HWI
267 >1 as a cut-off for hazy days for Beijing. We now use the HWI to calculate the frequency of
268 hazy and clear conditions for past and future using ERA-5 reanalysis and PPE members.

269 **4. Historical and future changes in the frequency of hazy and clear conditions**

270 The changes in the number of hazy and clear days per winter, as defined by HWI
271 thresholds, from the ERA-5 reanalyses and the PPE are shown in Fig. 4. For ERA-5, the
272 frequency of hazy days has increased, whereas the frequency of clear days has reduced for the
273 period 1979-2018. The mean frequency of hazy days using 16 PPE members shows a relatively
274 larger increase than ERA-5 for the same 1979-2018 time-period (Fig. 4a). In contrast, the mean
275 frequency of clear days from the PPE for this period shows a similar reduction to that obtained
276 using the ERA-5 reanalyses (Fig. 4b).



277 We examine the changes in the frequency of hazy and clear days for the historical
278 (1979-2005) and three future periods, i.e. near (2006-2032), mid (2033-2059) and far (2060-
279 2086) future. The mean frequency of hazy days is 14.7 days per winter obtained from the ERA-
280 5 reanalysis and 15.0 days per winter from the PPE mean for the historical period. The
281 corresponding values for clear days are 15.0 days and 15.2 days per winter for ERA-5 and PPE,
282 respectively. This shows a good agreement between the mean frequencies of hazy and clear
283 days for the ERA-5 data and the PPE mean for the historical period.



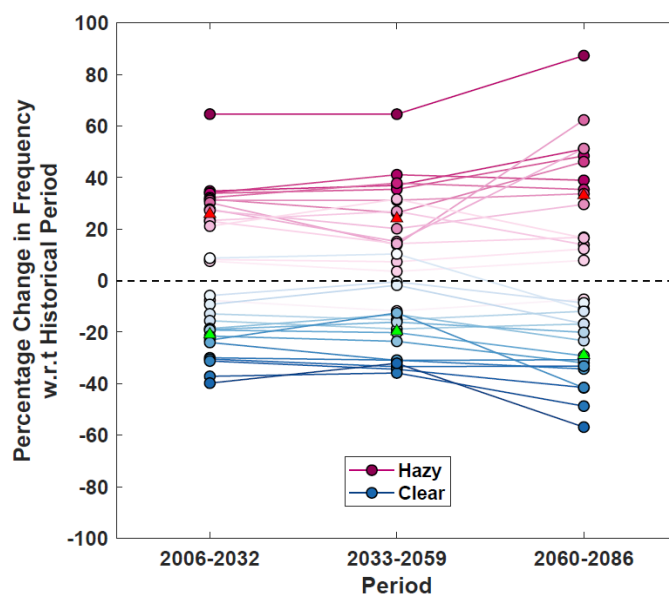
284

285 **Figure 4** Frequency of hazy (pink line) and clear days (blue line) per winter from ERA-5 reanalysis
286 (1979 to 2018). Year 1979 represents period from 1 December 1979 to 28 February 1980 and so on.
287 For each winter (DJF), we calculate the total number of hazy days with $HWI > 1$ and clear days with
288 $HWI < -1$. Grey lines show frequencies from 16 individual PPE members and black line shows the
289 mean of frequency using all 16 PPE members for 1969-2087 under the RCP8.5 scenario. Linear trend
290 is calculated using line of best fit.

291 The mean change in the frequency of hazy days averaging across all PPE members is
292 26%, 24% and 33% for the near, mid and far future respectively as compared to the historical
293 period, suggesting that the frequency of hazy days will likely increase for all future periods



294 (Fig. 5). However, there exists a very large range in the projected change for all three future
295 periods suggesting internal variability or parametric effect could influence the future
296 projections of haze conducive weather. For near and mid future, hazy days are projected to
297 change by -8% to 65% and -12% to 65% across the 16 PPE members, respectively, as compared
298 to the frequency for historical period. For far future, the range of projected change is even
299 larger, and an increase of ~87% in the frequency of hazy days is also possible. It should be
300 noted, for all three periods, only one of the sixteen ensemble members suggests a decrease in
301 daily haze frequency.



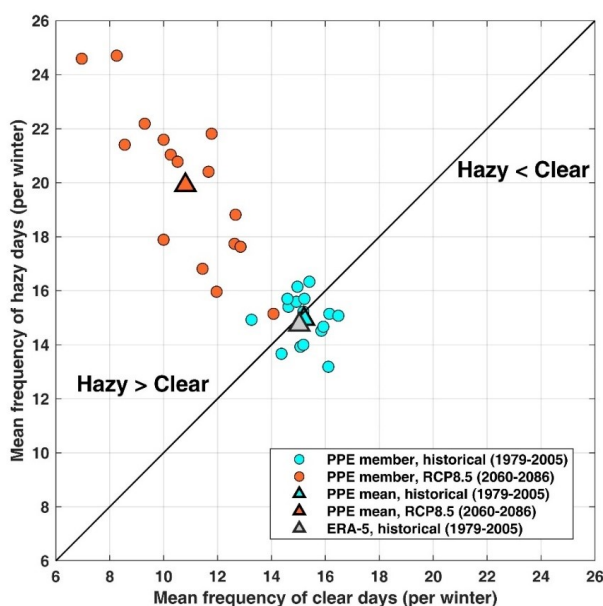
302

303 **Figure 5** Percentage change in the frequency of winter hazy and clear days averaged over the near
304 (2006-2032), mid (2033-2059) and far (2060-2086) futures under RCP8.5 as compared to the historical
305 period (1979-2005). The length of near, mid and far future is the same as historical (i.e. 27 years). Small
306 coloured circles (blue and pink) represent PPE members and triangles (red and green) represents the
307 mean of PPE members.

308 For the clear days, the mean change in the frequency of clear days averaging across all
309 PPE members is -21%, -20% and -29% for near, mid and far future, respectively (Fig 5).
310 Considering the range across the 16 PPE members, the frequency for near, mid and far future
311 is projected to change by -40% to 9%, -36% to 10% and -57% to -9%, respectively. Overall,



312 most ensemble members show an increase in the frequency of hazy days and a reduction in the
313 frequency of clear days for all three future periods however negligible change or even the
314 opposite change, though less likely, but possible for all periods.



315

316 **Figure 6** Frequency of winter hazy days versus clear days averaged over the historical period
317 (1979-2005) and the far-future (2060-2086) period under RCP8.5 using all PPE members.
318 Circles denote individual PPE members whereas triangles denote the mean of the members.
319 Grey triangle shows mean frequency from ERA-5 reanalysis for the historical period (1979-
320 2005). The black solid line shows the 1:1 (identity) line.

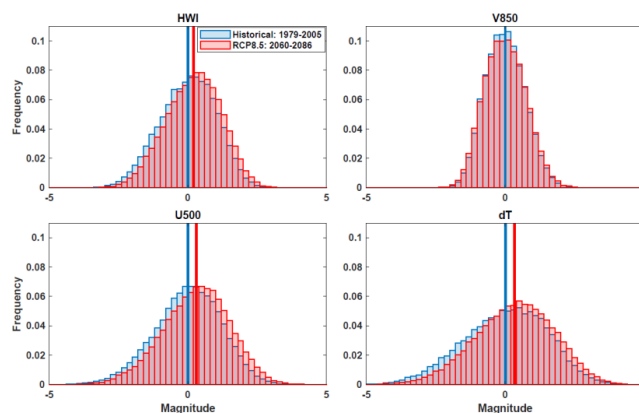
321 In addition to the changes in the frequencies over time, we also investigate the relative
322 changes in the frequency of hazy days versus clear days for a given winter. The average
323 frequency of hazy days and clear days over the historical period are almost equal for each PPE
324 member (Fig 6). All PPE members show higher frequency of hazy days than clear days under
325 the far future (2060-2085), however, there exists a substantial range in this change. The
326 frequency of winter haze days can be similar or up to 3.5 times the frequency of clear days
327 (Fig. 6). Similar results are also obtained for near and mid-future. Averaged across the PPE



328 members, the number of hazy days can increase by ~ 2 times as compared to the number of
329 clear days in future. As noted in Fig. 6, the spread in the frequency of hazy days amongst
330 individual ensemble members is also larger for the far future (2060-2086) compared to the
331 historical period. This suggests a larger uncertainty and a larger range of possible future
332 meteorological conditions affecting haze and air quality as compared to the historical period.
333 Other studies have (e.g., Cai et al., 2017; Callahan and Mankin, 2020) also found similar
334 increases in the frequency of hazy days for the future. However, the range of projected change
335 differ substantially across models as well as ensemble members. In our study, in addition to
336 the frequency of hazy days, we also evaluate the changes in the frequency of clear days across
337 different future periods and compared the relative changes in both the frequencies, which is not
338 examined in the past studies.

339 **5. Role of individual meteorological variables**

340 We now investigate the role of individual constituent meteorological variables in
341 driving the changes in the HWI between the far-future (2060-86) and the historical (1979-2005)
342 period. The probability distribution of the HWI shows a shift in the distribution towards higher
343 magnitudes for the far-future as compared to the historical period (Fig 8). This implies an
344 increased frequency in hazy days, as values with $\text{HWI} > 1$ increase. A similar shift is apparent
345 in the zonal-mean wind (U_{500}) and the vertical temperature profiles (dT), whereas no shift is
346 noted in V_{850} suggesting a relatively less important role of V_{850} in driving the future changes
347 in the HWI. We also find that the shift in the HWI as well as U_{500} and dT distribution is
348 consistent across the 16 PPE members and is continual over time from the historical to the far-
349 future period. Despite using a multimodel ensemble and a different time-period than used here,
350 similar result with a relatively larger shift in the PDFs of U_{500} and dT as compared to V_{850} can
351 also be noted in the Cai et al. (2017).



352

353 **Figure 7** Probability Distribution Functions (PDF) for the winter HWI, meridional winds at
354 850 hPa pressure level (V_{850}), zonal winds at 500 hPa pressure level (U_{500}) and temperature
355 gradient between the lower and upper troposphere (dT). PDFs are created using daily DJF
356 values for the historical (blue) and far-future (red) under RCP 8.5 by pooling in all 16 PPE
357 members. Blue and red solid lines show the mean values of the PDF for historical and far
358 future, respectively.

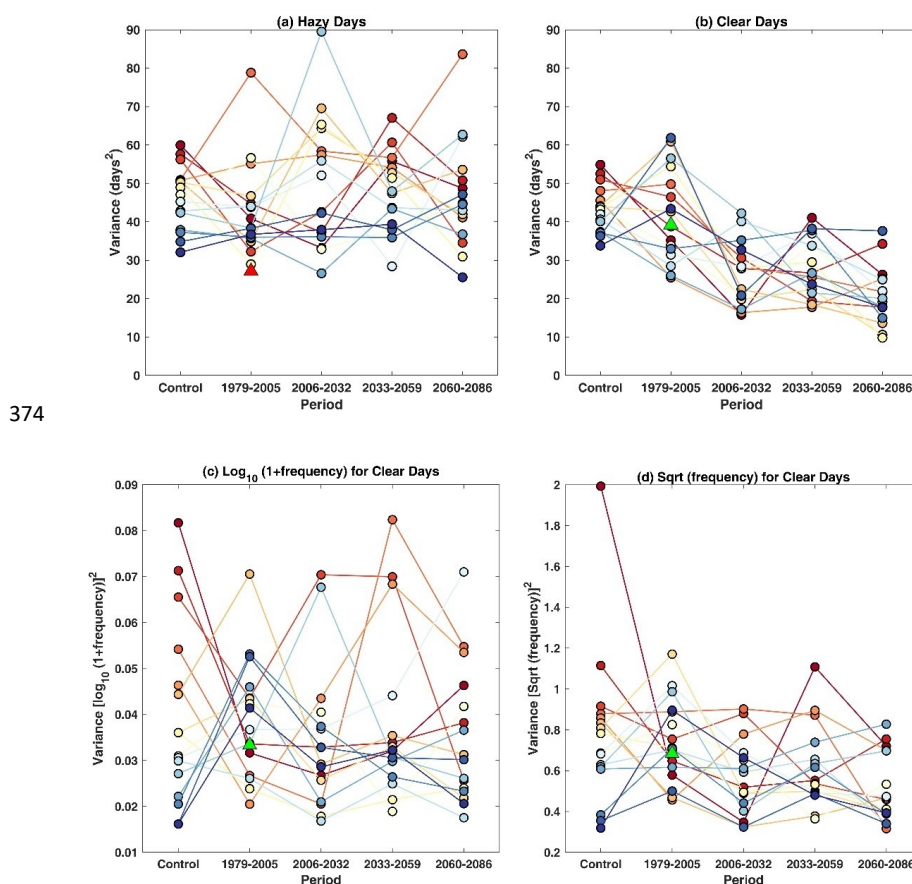
359 6. Interannual variability in the frequency of hazy and clear weather conditions

360 Large interannual variability in the frequency of hazy and clear days is apparent in both
361 individual PPE members and ERA-5 reanalysis (Section 4). Therefore, we examine the changes
362 in the interannual variance of the frequencies for future periods as compared to the historical
363 period. We also compare the variance in historical and future time-periods with the variance in
364 the control simulation to discern the influence of the model physical parameterisations, i.e.
365 parametric effect, on the variance.

366 The interannual variance for ERA-5 data is 27 days² and 39 days² for hazy and clear
367 days, respectively, for the historical period (1979-2005) (triangles in Fig. 8a-b). The
368 interannual variance in the frequency of hazy days derived from the PPE members for the
369 historical period is larger than that for the ERA-5, whereas for the clear days the variance for
370 ERA-5 lies within the range of the PPE members. No consistent change in the interannual
371 variance of hazy days is noted for any of the PPE members (note the changes in colour ranking)



372 from the historical to the future periods suggesting little influence of the parametric effect on
373 the interannual variance of hazy days.



376 **Figure 8** Interannual variance in frequency of winter (a) hazy and (b) clear days for the control
377 simulation, historical (1979-2005), and near (2006-2032), mid (2033-2059) and far-future (2060-2086)
378 under RCP8.5 for all 16 PPE members. Coloured circles are for individual PPE members and triangles
379 for ERA-5 reanalysis. (c-d) are same as (b) but with \log_{10} and square root power transformations. For
380 (c-d), we first calculate the \log_{10} of (1+frequency) and square-root of the frequency of clear days for the
381 control simulation and each time-period, and then estimate variance for each respective period. The
382 length of control simulation and all future periods is the same as historical, i.e. 27 years. The 27 years
383 used for control here are randomly selected from 170-year control simulation for each member.

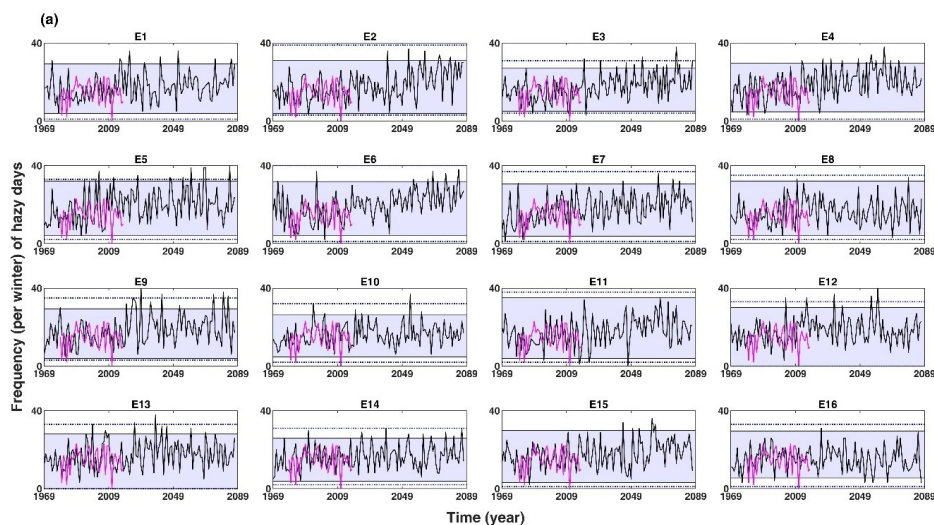
384 In contrast, the frequency of clear days for most PPE members show a marked reduction
385 in the interannual variance from historical to near-future (Fig. 8b). However, as the frequency
386 of clear days show a decreasing trend in time (see Fig. 4b), the mean frequency would be



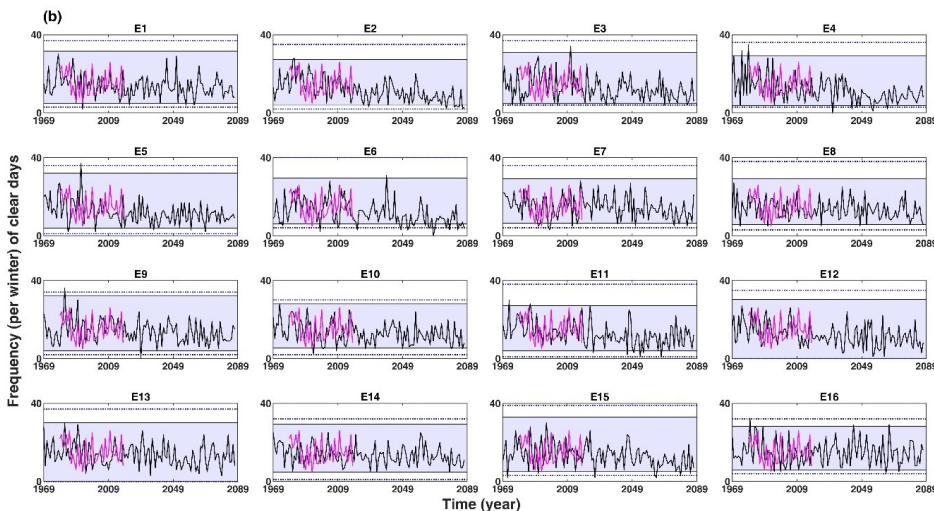
387 expected to reduce for the three future periods. Also, the reduction in variance could arise as
388 the frequencies of clear days approach their lower bound of zero. With count data, a power
389 transformation is often applied to stabilize the variance across all time periods. We tried two
390 power transformations, i.e. $\log_{10}(1+x)$ and square-root (x), where x is the count data (Fig. 8c-
391 d). We find the spread in the variance in the control simulation across the PPE members is
392 comparable with the historical as well as future periods (Fig. 8c-d). Note that for control
393 simulation we randomly selected 27 years (length same as historical and future periods) from
394 170 years of control simulation from each PPE member, however, we note comparable variance
395 for the other randomly selected samples. Figure 8 (c-d) also shows that the individual PPE
396 members show inconsistent changes in the variance (noting changes in the colour ranking)
397 from control to historical and future periods. Therefore, no robust changes in the interannual
398 variance of hazy or $\log_{10}(1 + \text{frequency of clear days})$ can be detected from control to historical
399 and future periods. This means we can use the variance in the control simulation as a
400 representative estimate of internal variability. This enables us to quantify the influence of the
401 parametric effect and anthropogenic climate change on the trends across the different periods
402 (see next section).

403 **7. Influence of the parametric effect and anthropogenic climate change on trends**

404 We discern the influence of the parametric effect and anthropogenic climate change on
405 the future projections of the trends in the frequency of hazy and clear days. Figure 9 shows the
406 time series of the frequency of winter hazy and clear days from ERA-5 and the 16 PPE
407 members for the historical and future periods. The 95th percentile values (blue shaded region)
408 and the range (blue dotted lines) in the frequency of hazy and clear days from the respective
409 control simulation for each PPE member are also shown.



410



411

412 **Figure 9** Frequency of (a) hazy and (b) clear days per winter for individual PPE members
413 (black line) under the historical and RCP8.5 scenarios for 1969-2087 and ERA5 reanalysis
414 (pink line) for 1979-2018. Blue shaded region shows the 95th confidence interval and blue
415 dashed line shows the range of the frequency of hazy and clear days for the pre-industrial
416 control simulation of 170-years.

417 For hazy days, the time series for selected PPE members (e.g. E3, E4) show increasing
418 positive trends. In particular towards the end of the 21st century (Fig. 9a), the lower half of the
419 control range is seldom sampled and more than the expected number of values lie above the

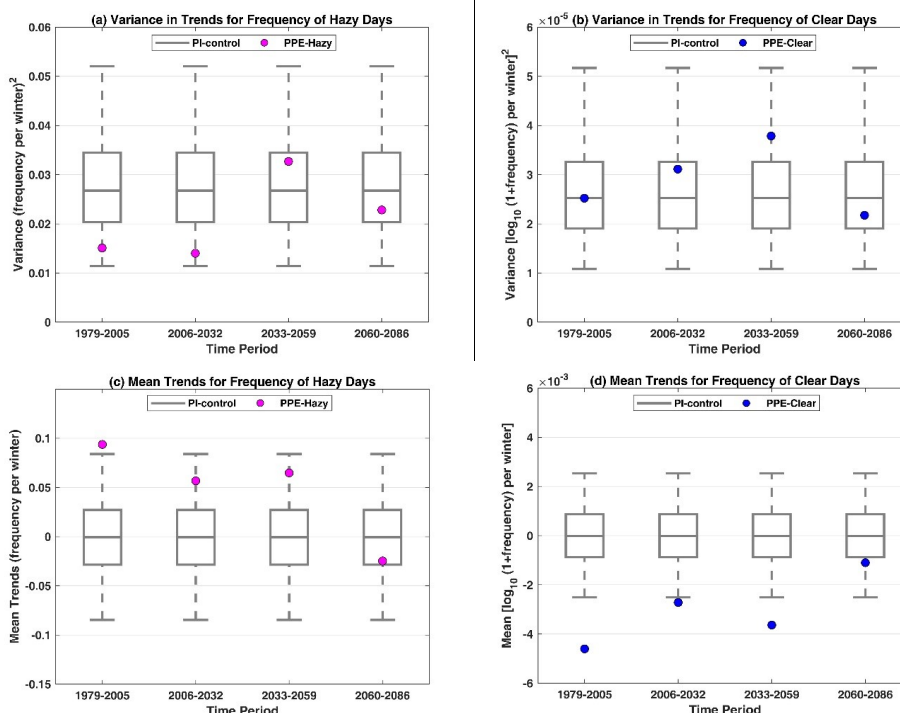


420 97.5th percentile of the control frequencies. In contrast, for other PPE members (e.g. E8, E10),
421 the full time series sample the control distribution evenly throughout the full period. For clear
422 days, some members (e.g. E3, E4) show a clear reduction during the 21st century whilst others
423 (e.g. E16) show that no trend and explore the control distribution evenly (Fig 9b).

424 We first examine the influence of the parametric effect on the trends in the frequency
425 of hazy and clear days. As can be noted in section 6, for hazy days and $\log_{10}(1 + \text{frequency of}$
426 $\text{clear days})$, the estimate of interannual variance from the control is representative of all time
427 periods and shows no discernible parametric effect. Therefore, we pool the 16 PPE control
428 simulations to sample the internal variability. In Fig. 10 (a) and (b), we show the variance in
429 trends for the time series resampled using the control simulation (see captions for details on
430 resampling). The grey box and whiskers show the 95th confidence interval of the control
431 variance used to represent the internal variability. The variance in PPE trends calculated using
432 16 PPE members for selected time periods is overlaid (circles). In Fig. 10 (a-b), if the variance
433 for historical or future periods lies outside the whiskers, we conclude an impact of the
434 parametric effect on the trends. Note that the variance in trends for clear days is in log-
435 transformed space. As can be seen in Fig. 10a and 10b, the variance in PPE trends for historical
436 and future periods lies within the envelope of the internal variability for both hazy and clear
437 days. Therefore, we do not find any discernible influence of the parametric effect on the trends
438 in the frequency of hazy and clear days.



439



440

Figure 10 Variance in PPE trends for the frequency of winter (a) hazy and (b) clear days. Circles show the variance in trends from 16 PPE members for the historical (1979-2005) and near (2006-2032), mid (2033-2059) and far (2060-2086) future under the RCP8.5 scenario. Grey box and whiskers show the distribution of 10,000 values of variance in trends sub-sampled from the control simulation. (c-d) same as (a-b) but variance is replaced by mean. For box and whiskers, we first randomly sampled 10,000 time series of length 27 years using 2704 years of pre-industrial control simulation and calculated 10,000 values of trends. We then randomly sub-sample 16 trends values from the 10,000 trend values and calculate the variance and mean of 16 trend values. The boxes are at 25th and 75th percentile and the whiskers at 2.5th and 97.5th percentile of mean and variance distribution. For clear days, the frequencies were transformed to log space by applying a power transformation of $\log_{10}(1+\text{frequency})$ before calculating trends.

454

We now examine the influence of anthropogenic climate change on the trends in the frequency of hazy and clear conditions. We calculate the mean trend obtained from the 16 individual PPE member trends (Fig. 10c-d), to determine the influence of climate change across selected time periods. The grey whiskers in Fig. 10 (c) and (d) cover the range of trends that can be explained by internal variability and any trend values lying outside the grey whiskers represent the influence of anthropogenic climate change.

459



460 The mean trend in the frequency of both hazy and clear days for the historical period
461 (1979-2005) lie outside the 95% confidence interval of the control simulations, suggesting a
462 substantial impact of anthropogenic climate change on the historical trends in the PPE.
463 Similarly, the mean trends for clear days for near (2006-2032) and mid future (2033-2059) lie
464 outside the 95% confidence interval of the control simulation. Thus, we find the impact of the
465 climate change on both hazy and clear days. However, it is only discernible for specific periods
466 due to the underlying large internal variability in the frequency of hazy and clear days.

467 **8. Conclusions**

468 In this study, we elucidate for the first time the influence of model physical
469 parametrisations, in addition to internal variability and climate change, on the future hazy and
470 clear weather conditions over the North China Plain (NCP) using the Perturbed Parameter
471 Ensemble (PPE) from the Met Office HadGEM3-GC3 model. We use a meteorology-based
472 daily Haze Weather Index (HWI), which has been previously used by a number of studies to
473 examine the winter (December-February) haze conducive weather conditions over Beijing. We
474 first identify the regional extent of the application of the HWI over China. We find that the
475 HWI can be used as an indicator of hazy and clear weather conditions for the entire NCP due
476 to the spatial coherence of regional meteorological conditions over this region.

477 The PPE shows that under the RCP8.5 scenario, the mean frequency of hazy days can
478 increase by up to ~65% in near (2006-2032) and mid (2033-2059) future and by ~87% in far-
479 future (2060-2086) as compared to the historical period (1979-2005). In contrast, the frequency
480 of clear days can reduce by up to ~40% in near and mid-future and by ~57% in far-future.
481 However, the opposite change of relatively lower magnitude or negligible change in frequency
482 of hazy and clear, though less likely, is possible. The absolute number of hazy days for the far
483 future can remain same or up to ~3.5 times higher than the clear days for any given winter.



484 There also exist a large interannual variability in the frequency of hazy and clear weather
485 conditions. However, no systematic change in the interannual variance of the frequency of hazy
486 or clear days is projected in future as compared to the historical period. We also find that the
487 future changes in hazy or clear weather conditions are largely influenced by changes in the
488 zonal wind component and strong vertical temperature gradient between the lower to upper
489 troposphere over the North China Plain. We do not find any discernible influence of the
490 parametric effect on the future projections of trends in the frequency of hazy and clear days.
491 However, we find the impact of anthropogenic climate change on the trends for both hazy and
492 clear days for historical and specific future periods, suggesting climate change can exacerbate
493 the increase in the number of hazy and the reduction in the number of clear days in future.

494 This study considers four atmospheric variables to examine the changes in future hazy
495 and clear weather conditions, however, other atmospheric variables (e.g., boundary layer
496 height) or processes may also influence the hazy or clear weather conditions. Furthermore,
497 even though our study shows the potential for an increase in hazy weather conditions and a
498 reduction in clear weather conditions for the future periods examined using the HWI, the
499 formation of haze also depends on future emissions of air pollutants and their precursors. If the
500 source emissions are cut-off or reduced in the future, the risk of haze formation would naturally
501 reduce. Nevertheless, the projections of changes in the frequency and interannual variance in
502 haze conducive weather conditions can be very useful for developing successful adaptation and
503 mitigation policies for the future that consider both emissions and climate change, and therefore
504 can be beneficial for near and long-term planning and decision-making in relation to improving
505 future PM_{2.5} air quality.

506 **Data Availability**



507 The Copernicus Climate Change Service (C3S) (2017): ERA5: Fifth generation of ECMWF
508 atmospheric reanalyses of the global climate data are available through Copernicus Climate
509 Change Service Climate Data Store (CDS) (<https://cds.climate.copernicus.eu/>). The PM2.5
510 concentrations for the US Embassy station in Beijing are archived at the following website
511 (<http://www.stateair.net/web/historical/1/1.html>). The haze weather index time series for PPE
512 and visibility data used in this paper can be obtained from the authors. The CAQRA dataset
513 can be freely downloaded at <https://doi.org/10.11922/sciencedb.00053>.

514 **Author Contribution**

515 SJ and RMD conceived and designed the manuscript; DS conducted PPE simulations using
516 Met Office HadGEM model; LP provided the visibility data; SJ performed data analysis,
517 produced figures, wrote the first draft; all co-authors provided comments on the manuscript
518 and contributed to writing.

519 **Competing interests**

520 The authors declare no financial or non-financial conflict of interest.

521 **Acknowledgements**

522 We thank Dr Li Ke for discussion on the HWI calculation and Dr Peiqun Zhang for discussion
523 on severe haze episodes in China. This work and its contributors (SJ, RMD, DS, ST, ZS) were
524 supported by the UK-China Research & Innovation Partnership Fund through the Met Office
525 Climate Science for Service Partnership (CSSP) China as part of the Newton Fund (Met Office
526 Reference Number: DN37368). RD and ZS also acknowledge NERC for funding under the
527 Atmospheric Pollution and Human Health Programme: Grant Nos. NE/N006941/1 and
528 NE/N007190/1. CL was supported by the National Key Research and Development Program
529 of China (Grant No. 2018YFA0606501).



530 **References**

- 531 An, Z., Huang, R. J., Zhang, R., Tie, X., Li, G., Cao, J., Zhou, W., Shi, Z., Han, Y., Gu, Z., and
532 Ji, Y.: Severe haze in northern China: A synergy of anthropogenic emissions and
533 atmospheric processes, *Proc Natl Acad Sci U S A*, 116, 8657-8666,
534 10.1073/pnas.1900125116, 2019.
- 535 Bai, N., Khazaei, M., van Eeden, S. F., and Laher, I.: The pharmacology of particulate matter
536 air pollution-induced cardiovascular dysfunction, *Pharmacology & therapeutics*, 113, 16-
537 29, 2007.
- 538 Cai, W., Li, K., Liao, H., Wang, H., and Wu, L.: Weather conditions conducive to Beijing
539 severe haze more frequent under climate change, *Nature Climate Change*, 7, 257-262,
540 10.1038/nclimate3249, 2017.
- 541 Callahan, C. W., Schnell, J. L., and Horton, D. E.: Multi-index attribution of extreme winter
542 air quality in Beijing, China, *Journal of Geophysical Research: Atmospheres*, 124, 4567-
543 4583, 2019.
- 544 Callahan, C. W., and Mankin, J. S.: The Influence of Internal Climate Variability on Projections
545 of Synoptically Driven Beijing Haze, *Geophysical Research Letters*, 47,
546 10.1029/2020gl088548, 2020.
- 547 Chen, H., and Wang, H.: Haze days in North China and the associated atmospheric circulations
548 based on daily visibility data from 1960 to 2012, *Journal of Geophysical Research:*
549 *Atmospheres*, 120, 5895-5909, 2015.
- 550 Deser, C., Knutti, R., Solomon, S., and Phillips, A. S.: Communication of the role of natural
551 variability in future North American climate, *Nature Climate Change*, 2, 775-779, 2012.
- 552 Deser, C., Phillips, A. S., Alexander, M. A., and Smoliak, B. V.: Projecting North American
553 climate over the next 50 years: Uncertainty due to internal variability, *Journal of Climate*,
554 27, 2271-2296, 2014.



- 555 Han, Z., Zhou, B., Xu, Y., Wu, J., and Shi, Y.: Projected changes in haze pollution potential in
556 China: an ensemble of regional climate model simulations, *Atmospheric Chemistry and*
557 *Physics*, 17, 10109-10123, 10.5194/acp-17-10109-2017, 2017.
- 558 Hawkins, E., and Sutton, R.: Time of emergence of climate signals, *Geophysical Research*
559 *Letters*, 39, n/a-n/a, 10.1029/2011gl050087, 2012.
- 560 He, J., Yu, Y., Xie, Y., Mao, H., Wu, L., Liu, N., and Zhao, S.: Numerical model-based
561 artificial neural network model and its application for quantifying impact factors of urban
562 air quality, *Water, Air, & Soil Pollution*, 227, 1-16, 2016.
- 563 Hersbach, H., Bell, B., Berrisford, P., Hirahara, S., Horányi, A., Muñoz-Sabater, J., Nicolas,
564 J., Peubey, C., Radu, R., Schepers, D., Simmons, A., Soci, C., Abdalla, S., Abellan, X.,
565 Balsamo, G., Bechtold, P., Biavati, G., Bidlot, J., Bonavita, M., Chiara, G., Dahlgren, P.,
566 Dee, D., Diamantakis, M., Dragani, R., Flemming, J., Forbes, R., Fuentes, M., Geer, A.,
567 Haimberger, L., Healy, S., Hogan, R. J., Hólm, E., Janisková, M., Keeley, S., Laloyaux,
568 P., Lopez, P., Lupu, C., Radnoti, G., Rosnay, P., Rozum, I., Vamborg, F., Villaume, S.,
569 and Thépaut, J. N.: The ERA5 global reanalysis, *Quarterly Journal of the Royal*
570 *Meteorological Society*, 146, 1999-2049, 10.1002/qj.3803, 2020.
- 571 Hong, C., Zhang, Q., Zhang, Y., Davis, S. J., Tong, D., Zheng, Y., Liu, Z., Guan, D., He, K.,
572 and Schellnhuber, H. J.: Impacts of climate change on future air quality and human health
573 in China, *Proceedings of the National Academy of Sciences*, 116, 17193-17200, 2019.
- 574 Hou, P., and Wu, S.: Long-term changes in extreme air pollution meteorology and the
575 implications for air quality, *Scientific reports*, 6, 1-9, 2016.
- 576 Jia, B., Wang, Y., Yao, Y., and Xie, Y.: A new indicator on the impact of large-scale circulation
577 on wintertime particulate matter pollution over China, *Atmospheric Chemistry and*
578 *Physics*, 15, 11919-11929, 2015.



- 579 Kan, H., London, S. J., Chen, G., Zhang, Y., Song, G., Zhao, N., Jiang, L., and Chen, B.:
580 Differentiating the effects of fine and coarse particles on daily mortality in Shanghai,
581 China, *Environment international*, 33, 376-384, 2007.
- 582 Kan, H., Chen, R., and Tong, S.: Ambient air pollution, climate change, and population health
583 in China, *Environment international*, 42, 10-19, 2012.
- 584 Kay, J. E., Deser, C., Phillips, A., Mai, A., Hannay, C., Strand, G., Arblaster, J. M., Bates, S.,
585 Danabasoglu, G., and Edwards, J.: The Community Earth System Model (CESM) large
586 ensemble project: A community resource for studying climate change in the presence of
587 internal climate variability, *Bulletin of the American Meteorological Society*, 96, 1333-
588 1349, 2015.
- 589 Knutti, R., Furrer, R., Tebaldi, C., Cermak, J., and Meehl, G. A.: Challenges in combining
590 projections from multiple climate models, *Journal of Climate*, 23, 2739-2758, 2010.
- 591 Kong, L., Tang, X., Zhu, J., Wang, Z., Li, J., Wu, H., Wu, Q., Chen, H., Zhu, L., and Wang,
592 W.: A 6-year-long (2013–2018) high-resolution air quality reanalysis dataset in China
593 based on the assimilation of surface observations from CNEMC, *Earth System Science*
594 *Data*, 13, 529-570, 2021.
- 595 Li, K., Liao, H., Cai, W., and Yang, Y.: Attribution of Anthropogenic Influence on
596 Atmospheric Patterns Conducive to Recent Most Severe Haze Over Eastern China,
597 *Geophysical Research Letters*, 45, 2072-2081, 10.1002/2017gl076570, 2018.
- 598 Li, Q., Zhang, R., and Wang, Y.: Interannual variation of the wintertime fog–haze days across
599 central and eastern China and its relation with East Asian winter monsoon, *International*
600 *Journal of Climatology*, 36, 346-354, 2016.
- 601 Liu, C., Zhang, F., Miao, L., Lei, Y., and Yang, Q.: Future haze events in Beijing, China: When
602 climate warms by 1.5 and 2.0°C, *International Journal of Climatology*, 40, 3689-3700,
603 10.1002/joc.6421, 2019.



- 604 Liu, Q., Jia, X., Quan, J., Li, J., Li, X., Wu, Y., Chen, D., Wang, Z., and Liu, Y.: New positive
605 feedback mechanism between boundary layer meteorology and secondary aerosol
606 formation during severe haze events, *Scientific reports*, 8, 1-8, 2018.
- 607 Liu, T., Gong, S., He, J., Yu, M., Wang, Q., Li, H., Liu, W., Zhang, J., Li, L., Wang, X., Li, S.,
608 Lu, Y., Du, H., Wang, Y., Zhou, C., Liu, H., and Zhao, Q.: Attributions of meteorological
609 and emission factors to the 2015 winter severe haze pollution episodes in China's Jing-
610 Jin-Ji area, *Atmospheric Chemistry and Physics*, 17, 2971-2980, 10.5194/acp-17-2971-
611 2017, 2017.
- 612 Pei, L., Yan, Z., Sun, Z., Miao, S., and Yao, Y.: Increasing persistent haze in Beijing: potential
613 impacts of weakening East Asian winter monsoons associated with northwestern Pacific
614 sea surface temperature trends, *Atmospheric Chemistry and Physics*, 18, 3173-3183,
615 2018.
- 616 Pendergrass, D., Shen, L., Jacob, D., and Mickley, L.: Predicting the impact of climate change
617 on severe wintertime particulate pollution events in Beijing using extreme value theory,
618 *Geophysical Research Letters*, 46, 1824-1830, 2019.
- 619 Petäjä, T., Järvi, L., Kerminen, V.-M., Ding, A., Sun, J., Nie, W., Kujansuu, J., Virkkula, A.,
620 Yang, X., and Fu, C.: Enhanced air pollution via aerosol-boundary layer feedback in
621 China, *Scientific reports*, 6, 1-6, 2016.
- 622 Qiu, L., Yue, X., Hua, W., and Lei, Y.-D.: Projection of weather potential for winter haze
623 episodes in Beijing by 1.5 °C and 2.0 °C global warming, *Advances in Climate Change*
624 *Research*, 11, 218-226, 10.1016/j.accre.2020.09.002, 2020.
- 625 Renhe, Z., Li, Q., and Zhang, R.: Meteorological conditions for the persistent severe fog and
626 haze event over eastern China in January 2013, *Science China Earth Sciences*, 57, 26-35,
627 2014.



- 628 Sexton, D. M., McSweeney, C. F., Rostron, J. W., Yamazaki, K., Booth, B. B., Murphy, J. M.,
629 Regayre, L., Johnson, J. S., and Karmalkar, A. V.: A perturbed parameter ensemble of
630 HadGEM3-GC3. 05 coupled model projections: part 1: selecting the parameter
631 combinations, *Climate Dynamics*, 56, 3395-3436, 2021.
- 632 Shen, L., Jacob, D. J., Mickley, L. J., Wang, Y., and Zhang, Q.: Insignificant effect of climate
633 change on winter haze pollution in Beijing, *Atmospheric Chemistry and Physics*, 18,
634 17489-17496, 10.5194/acp-18-17489-2018, 2018.
- 635 Sun, Y., Jiang, Q., Wang, Z., Fu, P., Li, J., Yang, T., and Yin, Y.: Investigation of the sources
636 and evolution processes of severe haze pollution in Beijing in January 2013, *Journal of*
637 *Geophysical Research: Atmospheres*, 119, 4380-4398, 2014.
- 638 Tie, X., Huang, R.-J., Cao, J., Zhang, Q., Cheng, Y., Su, H., Chang, D., Pöschl, U., Hoffmann,
639 T., and Dusek, U.: Severe pollution in China amplified by atmospheric moisture,
640 *Scientific Reports*, 7, 1-8, 2017.
- 641 Wang, J.-L., Zhang, Y.-h., Shao, M., Liu, X.-l., Zeng, L.-m., Cheng, C.-l., and Xu, X.-f.:
642 Quantitative relationship between visibility and mass concentration of PM_{2.5} in Beijing,
643 *Journal of environmental sciences*, 18, 475-481, 2006.
- 644 Wang, L., Wei, Z., Yang, J., Zhang, Y., Zhang, F., Su, J., Meng, C., and Zhang, Q.: The 2013
645 severe haze over southern Hebei, China: model evaluation, source apportionment, and
646 policy implications, *Atmospheric Chemistry and Physics*, 14, 3151-3173, 2014a.
- 647 Wang, Y., Yao, L., Wang, L., Liu, Z., Ji, D., Tang, G., Zhang, J., Sun, Y., Hu, B., and Xin, J.:
648 Mechanism for the formation of the January 2013 heavy haze pollution episode over
649 central and eastern China, *Science China Earth Sciences*, 57, 14-25, 2014b.
- 650 Xu, M., Chang, C. P., Fu, C., Qi, Y., Robock, A., Robinson, D., and Zhang, H. m.: Steady
651 decline of east Asian monsoon winds, 1969–2000: Evidence from direct ground
652 measurements of wind speed, *Journal of Geophysical Research: Atmospheres*, 111, 2006.



- 653 Xu, P., Chen, Y., and Ye, X.: Haze, air pollution, and health in China, *Lancet*, 382, 2067,
654 10.1016/S0140-6736(13)62693-8, 2013.
- 655 Yamazaki, K., Sexton, D. M., Rostron, J. W., McSweeney, C. F., Murphy, J. M., and Harris,
656 G. R.: A perturbed parameter ensemble of HadGEM3-GC3. 05 coupled model
657 projections: part 2: global performance and future changes, *Climate Dynamics*, 56, 3437-
658 3471, 2021.
- 659 Yin, Z., and Wang, H.: Role of atmospheric circulations in haze pollution in December 2016,
660 *Atmospheric Chemistry and Physics*, 17, 11673-11681, 10.5194/acp-17-11673-2017,
661 2017.
- 662 Zhang, Q., Ma, Q., Zhao, B., Liu, X., Wang, Y., Jia, B., and Zhang, X.: Winter haze over North
663 China Plain from 2009 to 2016: Influence of emission and meteorology, *Environ Pollut*,
664 242, 1308-1318, 10.1016/j.envpol.2018.08.019, 2018.
- 665 Zhang, R., Jing, J., Tao, J., Hsu, S.-C., Wang, G., Cao, J., Lee, C. S. L., Zhu, L., Chen, Z., and
666 Zhao, Y.: Chemical characterization and source apportionment of PM 2.5 in Beijing:
667 seasonal perspective, *Atmospheric Chemistry and Physics*, 13, 7053-7074, 2013.
- 668 Zhang, L., Wilcox, L. J., Dunstone, N. J., Paynter, D. J., Hu, S., Bollasina, M., ... & Zou, L.
669 (2021). Future changes in Beijing haze events under different anthropogenic aerosol
670 emission scenarios. *Atmospheric Chemistry and Physics*, 21(10), 7499-7514.
- 671 Zhang, Z., Gong, D., Mao, R., Kim, S. J., Xu, J., Zhao, X., and Ma, Z.: Cause and predictability
672 for the severe haze pollution in downtown Beijing in November-December 2015, *Sci*
673 *Total Environ*, 592, 627-638, 10.1016/j.scitotenv.2017.03.009, 2017.
- 674
- 675